Dynamic Study of Highly Efficient CdS/CdSe Quantum Dot-Sensitized Solar Cells Fabricated by Electrodeposition

Xiao-Yun Yu, Jin-Yun Liao, Kang-Qiang Qiu, Dai-Bin Kuang,* and Cheng-Yong Su

MOE Key Laboratory of Bioinorganic and Synthetic Chemistry, KLGHEI of Environment and Energy Chemistry, State Key Laboratory of Optoelectronic Materials and Technologies, School of Chemistry and Chemical Engineering, Sun Yat-sen University, Guangzhou 510275, P. R. China

ABSTRACT

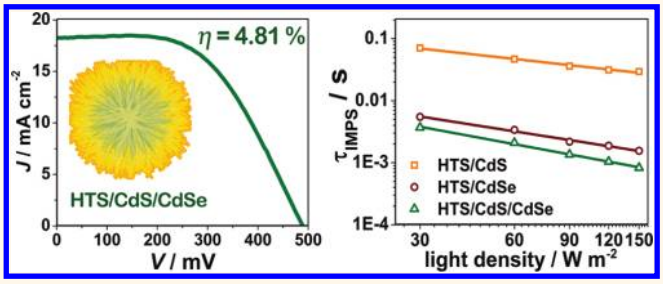

An *in situ* electrodeposition method is described to fabricate the CdS or/and CdSe quantum dot (QD) sensitized hierarchical TiO_2 sphere (HTS) electrodes for solar cell application. Intensity modulated photocurrent spectroscopy (IMPS), intensity modulated photovoltage spectroscopy (IMVS) and electrochemical impedance spectroscopy (EIS) measurements are performed to investigate the electron transport and recombination of quantum dot-sensitized solar cells (QDSSCs) based on HTS/CdS, HTS/CdSe, and HTS/CdS/CdSe photoelectrodes. This dynamic study reveals that the CdSe/CdS cosensitized solar cell performs ultrafast electron transport and high electron collection efficiency (98%). As a consequence, a power conversion efficiency as high as 4.81% (J_{SC} = 18.23 mA cm^{-2}, V_{OC} = 489 mV, FF = 0.54) for HTS/CdS/CdSe photoelectrode based QDSSC is observed under one sun AM 1.5 G illumination (100 mW cm^{-2}).

KEYWORDS: CdS · CdSe · quantum dot-sensitized solar cell · electrodeposition · intensity modulated photocurrent spectroscopy (IMPS) · intensity modulated photovoltage spectroscopy (IMVS) · electrochemical impedance spectroscopy (EIS)

Semiconductor quantum dots (QDs), which have extraordinary optical and electrical properties, could be viable alternatives to ruthenium complexes or organic dyes in sensitized solar cell applications.[1,2] Their unique band character,[2,3] high extinction coefficients[4,5] and impact ionization effects[6,7] suggest that QD materials are promising light absorbers for quantum dot-sensitized solar cells (QDSSCs). While initially demonstrating low efficiency for solar energy conversion,[8] the power conversion efficiency of QDSSCs has grown rapidly to over 4% in the past few years,[9−11] pointing to the intriguing possibility of attaining similar levels to those of dye-sensitized solar cells (DSSCs). QDSSCs remain far from optimized. Breakthroughs with regards to conversion efficiencies for QDSSCs might be realized through one of the following avenues: (i) an efficient method to control the QD size and size distribution or (ii) optimization of QD sensitized electrode structure, including integration of a suitable wide band gap matrix, high coverage, and band alignment of QDs, which will benefit both electron transfer and collection.

The preparation of QD sensitized electrodes, reported up to this point, can mainly be divided into one of two strategies. The first is the *in situ* growth of QDs onto metal oxide matrix through the chemical bath deposition (CBD)[12,13] or the successive ionic layer adsorption and reaction (SILAR)[14,15] method. This time-consuming strategy provides high coverage and direct attachment of QDs onto the substrate, resulting in high power conversion efficiencies.[16] The second strategy is the linking of the presynthesized colloidal QDs onto the matrix by linker-assisted adsorption (LA)[17−19] or *via* the direct adsorption (DA)[13] method. This inefficient strategy ensures good QD quality but is hindered by very low surface coverage, resulting in photovoltaic performances of less than 2.02%.[13,16] Recently, a hot-injection *in situ* growth of QDs onto TiO_2 films has been developed by Acharya *et al.*[20] We have reported a CdTe/CdS QD sensitized solar cell with a power conversion efficiency of 3.8%, prepared through a one-step linker-assisted chemical bath deposition (LACBD).[21] The electrodeposition method has been well developed for the fabrication of semiconductor hybrid materials for photoelectrochemical cell applications, and typically have the metal oxide/CdX (X = S, Se, or Te) core/shell structure.[22−24] Although the electrodeposition method is expected to perform

* Address correspondence to kuangdb@mail.sysu.edu.cn.

Received for review July 3, 2011 and accepted October 27, 2011.

Published online October 28, 2011
10.1021/nn203375g

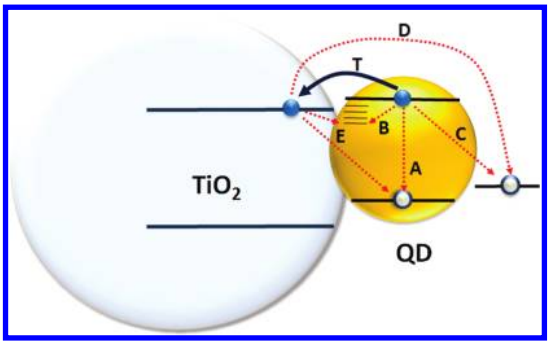

Scheme 1. Electron transport and charge recombination processes in QDSSCs. (A) recombination of electron in the QD conduction band and hole in the QD valence band; (B) trapping of the exited electrons by the surface states of QDs; recombination of the hole acceptors in the electrolyte and electrons in QDs (C) or TiO_2 (D); (E) back electron injection from TiO_2 to QDs; and (T) electron injection from QDs to TiO_2 crystalline.

well in the preparation of QD sensitized electrodes for QDSSC applications, little research has been reported thus far.

The processes of electron transfer in QDSSCs can be simplified as shown in Scheme 1. The dynamic study of the electron injection process (process **T**, the injection time is in the range of 10^{-8}—10^{-10} s) can be carried out by transient fluorescence spectroscopy.[25,26] Recombination of electrons in TiO_2 and holes (*e.g.*, I_3^-) in the electrolyte (process **D**) is the main electron loss pathway in DSSCs.[8] Compared to DSSCs, the recombination in QDSSCs is more complicated with five major pathways (**A**—**E**). Process **D** relates directly to the coverage of QDs on the TiO_2 surface. Additionally, the electron quenching, trapping, and recombining with the electrolyte (processes **A**, **B**, and **C**, respectively) strongly depends on the quality of QDs.[27] Besides, electrons injected into TiO_2 have the possibility of feeding back to QDs (process **E**),[8] and later either trapped by the QD surface states or recombined directly with the holes in the QD valence band. To evaluate these recombination processes in QDSSCs, the electrochemical impedance spectroscopy (EIS) measurements were successfully carried out in many cases.[16,28] In addition, intensity modulated photocurrent spectroscopy (IMPS) and intensity modulated photovoltage spectroscopy (IMVS) have also been widely employed to estimate the electron dynamic responses in DSSCs,[29,30] in which a small sinusoidal perturbation is superimposed upon a strong DC light illumination. The IMPS (or IMVS) measures the photocurrent (or photovoltage) at short circuit (or open circuit) condition under a modulated incident light illumination. The photocurrent and photovoltage responses are used to evaluate the time constant for the electron transport and recombination processes in sensitized solar cells, respectively.[31,32] However, according to our knowledge, no data of their utilization in QDSSCs have been reported.

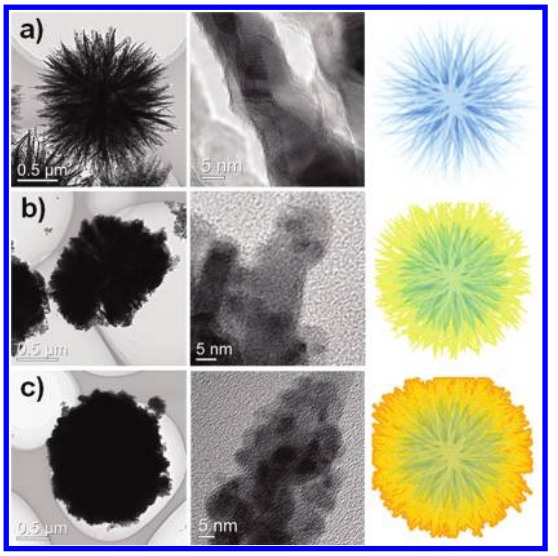

Figure 1. TEM image (left), HRTEM image (middle), and schematic figure (right) of as-prepared HTS (a); HTS/CdS (b); and HTS/CdS/CdSe (c).

In the present work, a convenient electrodeposition method to synthesis CdS, CdSe, and CdS/CdSe quantum dots on the hierarchical TiO_2 spheres (HTS) consisting of nanorods and nanoparticles has been demonstrated. Caused by the compact covering of QDs on HTS, the power conversion efficiency of QDSSCs has evidently been improved. The highest power conversion efficiency of QDSSCs reaches 4.81% for HTS/CdS/CdSe photoelectrode under one sun illumination. Furthermore, for the first time, the IMPS and IMVS measurements have been employed here to evaluate the electron transport and charge recombination processes. The results reflect the differences in electron transport and recombination characteristics of QDSSCs based on HTS/CdS, HTS/CdSe, or HTS/CdS/CdSe photoelectrode, which directly affects the photocurrent and power conversion efficiency. In addition, the conventional EIS characterization was also carried out to verify the recombination result as compared to that obtained from the IMVS measurement.

RESULTS AND DISCUSSION

The hierarchical TiO_2 sphere (HTS) material in the anatase phase was synthesized according to our previous work.[33] The TiO_2 spheres constructed of nanorods and nanoparticles were in the average size of 2.1 μm, as shown in Figure 1a. This unique architecture has several advantages of large surface area, fast electron transportation, and outstanding light-scattering ability.[33] The HTS-FTO electrodes were prepared by a screen printing method and later immersed in the Cd-containing electrolyte. The electrodeposition processes of CdS or CdSe QDs were carried out with constant current using a Pt counter-electrode. Scheme 2 illustrates the experimental diagram of depositing CdSe QDs onto the as-prepared HTS/CdS electrode.

The CdS QD fabrication was accomplished in a similar system using Cd^{2+} and thiourea as precursors. The electrodeposition of CdS has deposited QDs on the surface of TiO_2 nanorods and nanoparticles in HTS (Figure 1b). However, the nanorods of HTS can still be distinguished in the TEM image (Figure 1b, left). HR-TEM (Figure 1b, middle) shows that CdS QDs with sizes of around 4.5 ± 0.5 nm have covered the TiO_2 nanorod, yet a large amount of exposed TiO_2 can still be observed. When CdSe was further deposited on the HTS/CdS electrode, the interspace in HTS was compactly filled with a large number of CdSe QDs (8.0 ± 0.7 nm in size), as shown in Figure 1c. The peak corresponds to the (220) plane of cubic CdS and/or cubic CdSe can be clearly detected (JCPDS No. 65-2887 and 65-2891, respectively) in XRD patterns, showing that both the CdS and CdSe QDs prepared by electrodeposition are of the zinc blend structure (Figure S1, Supporting Information).

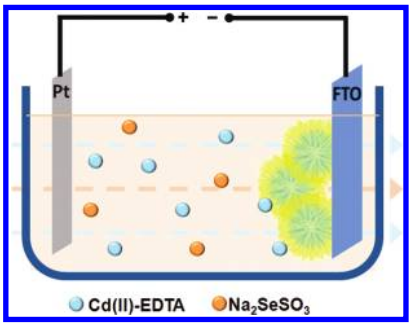

Scheme 2. Experimental system and electrodeposition process of depositing CdSe QDs onto as-prepared HTS/CdS electrode with Cd(II)-EDTA and Na_2SeSO_3 as precursors.

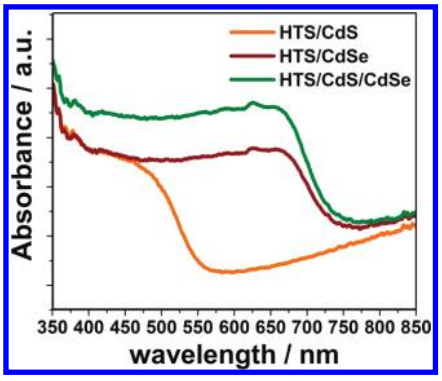

Figure 2. UV−vis absorption spectra of CdS, CdSe, and CdS/CdSe QD sensitized on HTS electrodes.

The UV−vis absorption spectra of CdS or/and CdSe QD-sensitized HTS electrodes are shown in Figure 2. The absorption onset position of the HTS/CdS electrode is located at ~550 nm, while it red-shifts to ~730 nm for the HTS/CdSe electrode, ascribed to the band gap of CdSe being narrower than CdS.[2] In the case of the HTS/CdS/CdSe electrode, the absorption range remains the same with the CdSe sensitized electrode. However, the CdS and CdSe QD cosensitized structure enhances the absorption intensity in the whole UV−visible region. It is reasonable to propose that CdS could have a similar role as the ZnS layer, which leads to an increase in light absorption due to the loss of quantum confinement.[16]

The light conversion properties of QDSSCs based on these three photoelectrodes (HTS/CdS, HTS/CdSe, and HTS/CdS/CdSe) were characterized as current density−voltage curves ($J-V$, shown in Figure 3a), while the details of short circuit current density (J_{SC}), open circuit voltage (V_{OC}), fill factor (FF) and power conversion efficiency (η) are listed in Table 1. The HTS/CdS QDSSC shows the lowest J_{SC} and η due to the poor light absorption in a narrow region. The J_{SC} increases obviously for HTS/CdSe and HTS/CdS/CdSe QDSSCs, accompanied by an apparent enhancement of FF value. As a result, the power conversion efficiency more than doubled for HTS/CdSe QDSSCs, while an outstanding η of 4.81% was observed for HTS/CdS/CdSe cosensitized solar cells under one sun illumination (100 mW cm^{-2}). The incident-photon-to-current conversion efficiency (IPCE) curves in Figure 3b clearly illustrate that the

TABLE 1. Photovoltaic Parameters of QDSSCs Based on HTS/CdS, HTS/CdSe and HTS/CdS/CdSe Photoelectrodes Derived from Figure 3a

photoelectrode	J_{SC} (mA cm^{-2})	V_{OC} (mV)	η (%)	FF
HTS/CdS	7.53	492	1.01	0.27
HTS/CdSe	10.93	486	2.69	0.51
HTS/CdS/CdSe	18.23	489	4.81	0.54

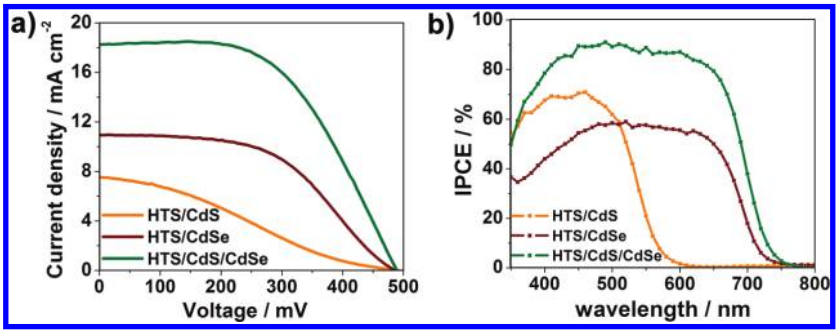

Figure 3. (a) $J-V$ and (b) IPCE curves of QDSSCs based on HTS/CdS, HTS/CdSe, and HTS/CdS/CdSe photoelectrodes assembled by polysulfide electrolyte and Pt counter-electrode.

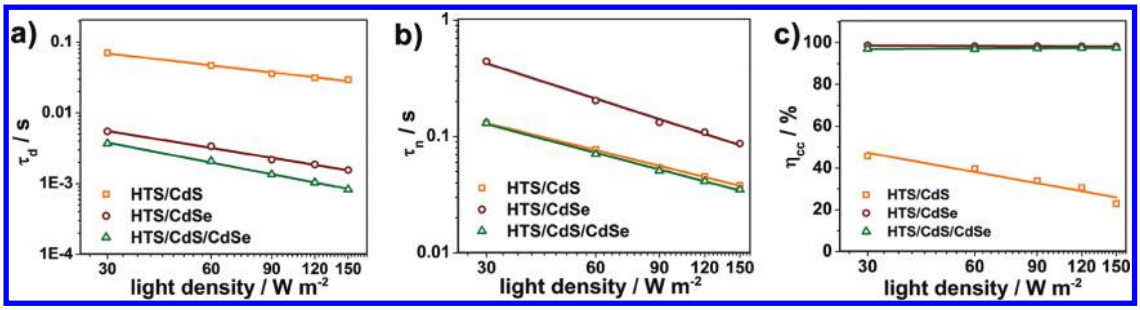

Figure 4. (a) Electron transit time, (b) electron lifetime, and (c) charge collection efficiency measured by IMPS or IMVS at different light densities for HTS/CdS, HTS/CdSe and HTS/CdS/CdSe QDSSCs.

active photon-to-current responses of HTS/CdSe and HTS/CdS/CdSe QDSSCs have red-shifted as compared to HTS/CdS QDSSC. The IPCE value of HTS/CdS/CdSe QDSSC exceeds 60% in the wide wavelength range of 400−680 nm, which correlate well with the UV−vis absorption and *J*−*V* results.

Intensity modulated photocurrent spectroscopy (IMPS)[34] and intensity modulated photovoltage spectroscopy (IMVS)[35] have been used as powerful tools to study the electron transport and recombination in DSSCs. However, no such systematic studies have been performed for QDSSCs. The electron transit time τ_d (or lifetime τ_n) can be calculated by expression $\tau_d = {}^1/_{2\pi f_{IMPS}}$ (or $\tau_n = {}^1/_{2\pi f_{IMVS}}$), where f_{IMPS} (or f_{IMVS}) is the frequency of the minimum IMPS (or IMVS) imaginary component, same as the expression used in DSSCs.[36,37] As shown in Figure 4 panels a and b, both the electron transit time and the lifetime decrease with the increase of light intensity.

The IMPS results (Figure 4a) at varied light intensities clearly illustrate that the τ_d for HTS/CdS/CdSe QDSSC (about 0.5−3.5 ms) is shorter than that for HTS/CdSe solar cell (1.5−5.5 ms), while the τ_d of HTS/CdS solar cell (29−70 ms) is the longest. This fact reveals that the electron transport rate in HTS follows the order of HTS/CdS/CdSe > HTS/CdSe ≫ HTS/CdS, which is a consequence of the following facts: (i) The higher intensity and red shift of light absorption in 400−750 nm increase the electron concentration in the TiO_2 substrate of HTS/CdS/CdSe and HTS/CdSe QDSSCs compared to HTS/CdS QDSSC, which directly accelerates the electron transport in TiO_2 and transfers to FTO glass. (ii) In the present QDSSCs with polysulfide electrolyte, the HTS/CdSe structure can provide a larger driving force for photogenerated electron injection than the HTS/CdS structure. Although the conduction band (CB) energies of CdS and CdSe are −0.8 V and −0.6 V (*vs* normal hydrogen electrode, NHE), respectively, in neutral solution,[38,39] they shift to −1.0 V and −1.2 V (*vs* NHE), respectively, when left in contact with polysulfide electrolyte (1 M Na_2S, 1 M S).[38,40] As a result, when compared to CdS QDs, the more negative conductive band energy level of CdSe QDs offers a larger driving force for electron transfer to the HTS substrate. (iii)

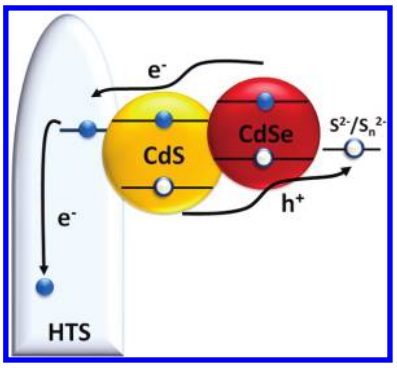

Scheme 3. Injection of photo-generated electron from CdSe QDs through CdS to HTS, and transportation of the injected electron in the one dimensional nanorod of HTS.

Because of the band edge shift in sulfide-containing electrolyte, the HTS/CdS/CdSe cosensitized solar cell with step-like band edge structure is more efficient in enlarging the charge separation in the QDs as compared to HTS/CdS or HTS/CdSe alone, as demonstrated in Scheme 3. In other words, the shunting of the electrons and holes in different directions accelerates the electron transport in the TiO_2 electrode. Furthermore, the substrate HTS with one-dimensional TiO_2 nanorods allows electron transport without obstruction in a certain range, which provides an important factor in the fast electron transit in the QDSSCs.[33]

Electron lifetime derived from IMVS (Figure 4b) reflects the recombination processes in QDSSCs shown in Scheme 1. Among the pathways, process **A** can be ignored in the QD sensitized TiO_2 system due to the highly efficient charge separation, while the other recombination processes (**B**−**E**) are affected by various factors. In Figure 4b, the HTS/CdSe QDSSC shows the longest electron lifetime. It is well-known that the charge recombination process **D** can be sharply diminished by improving QD coverage of the TiO_2 surface. The HTS/CdSe electrode obtained by electrodeposition of CdSe enhances the amount of QDs on HTS when compared to the HTS/CdS electrode (TEM observation, data not shown), thus blocking the recombination process **D** in HTS/CdSe QDSSCs, showing that the latter has left a large portion of TiO_2 surface exposed in the electrolyte (Figure 1b, left and middle images), and

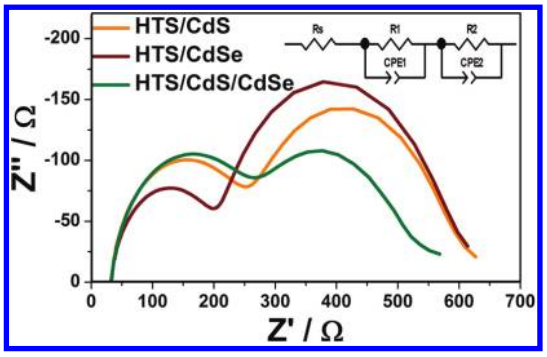

Figure 5. EIS spectra of QDSSCs based on HTS/CdS, HTS/CdSe, and HTS/CdS/CdSe electrodes measured in the dark at −0.5 V bias. The inset illustrates the equivalent circuit simulated to fit the impedance spectroscopy. R_1 and CPE_1 represent the charge transfer resistance and capacitance at electrolyte/counter electrode interface, respectively, while R_2 and CPE_2 represent the recombination resistance and capacitance at the TiO_2−QD/electrolyte interface, respectively.

therefore led to faster recombination rate of electrons in TiO_2 with polysulfide electrolyte. Hence, process **D** becomes the most important factor for the electron lifetime in HTS/CdS QDSSCs.

However, for HTS/CdS/CdSe cosensitized solar cell, the electron lifetime stays at the same level for HTS/CdS QDSSC. After the surface of HTS has been fully covered by QDs, the aggregation of CdSe QDs can be observed in the TEM image (Figure 1c). Then, the primary recombination process changes from the TiO_2-electrolyte (process **D**) to the one within QDs and QD-electrolyte,[28] as illustrated in processes **B** and **C** in Scheme 1. The boundary of semiconductor QDs may cause more electron trapping or reaction with the electrolyte before the electrons inject into TiO_2.[13,41] Therefore, the aggregation of CdS and CdSe QDs on HTS electrode may lead to faster charge recombination for HTS/CdS/CdSe QDSSC comparing to HTS/CdSe QDSSC.

The charge collection efficiency (η_{cc}) of QDSSCs in Figure 4c can be estimated by the IMPS and IMVS measurements and calculated by the expression: $\eta_{cc} = 1 - \tau_d/\tau_n$,[31,42] where the τ_d and the τ_n value are derived from Figure 4 panels a and b. In the expression $J_{SC} = q\eta_{lh}\eta_{inj}\eta_{cc}I_0$[43] ($q$ is the elementary charge, I_0 is the incident photon flux, η_{lh} is the light harvesting efficiency, η_{inj} is the electron injection efficiency, and η_{cc} is the charge collection efficiency), where J_{SC} is directly proportional to η_{cc} of sensitized solar cells, the decrease of η_{cc} of HTS/CdS QDSSC from 50% to 25% with the increase of light intensity associates directly to its low J_{SC}, resulting in the low power conversion efficiency of CdS sensitized solar cell. As for HTS/CdSe and HTS/CdS/CdSe QDSSCs, the η_{cc} are both of 98 ± 1% under varied light intensities, and hence prominent photovoltaic performance can be obtained. The results denote that the relatively fast recombination rate of HTS/CdS/CdSe QDSSC has been balanced by the fast electron transport. The difference of J_{SC} based on HTS/CdSe and HTS/CdS/CdSe electrodes is ascribed to η_{lh} and η_{inj}. Higher η_{lh} for the latter has been confirmed by the UV−vis absorption spectra. The step-like band edge structure is in favor of the electron and hole separation, and hence higher η_{inj} for HTS/CdS/CdSe is expected. Hereby, we conclude that J_{SC} and η of QDSSCs are affected by three factors: (i) light absorption intensity determined by both the QD material and the amount of loading; (ii) electron transport influenced by the band edge position and electron concentration; (iii) charge recombination rate.

TABLE 2. Simulated Values of Resistance (R) and Capacitance (CPE) of EIS Spectra Calculated by Equivalent Circuit as Shown in Figure 5. The Electron Lifetimes τ_n' Are Estimated by R_2 and CPE_2

photoelectrode	R_s (Ω)	R_1 (Ω)	CPE_1 (μF)	R_2 (Ω)	CPE_2 (μF)	τ_n' (ms)
HTS/CdS	31.2	247	21.7	378	494	187
HTS/CdSe	31.6	197	32.8	391	657	257
HTS/CdS/CdSe	33.5	258	26.4	360	484	174

It is worthy of notice that the η_{cc} of 98% of QDSSCs fabricated by the present electrodeposition method is much higher than that by the CBD method (about 55%) reported in the earlier article.[13] Combined with the aforementioned higher QD coverage, it reveals that the *in situ* electrodeposition fabrication of QD-sensitized TiO_2 electrode can avoid both the common low coverage (by the LA or DA method) and low electron collection efficiency (by the CBD method) drawbacks, providing a new strategy and solution to efficient QDSSCs.

Electrochemical impedance spectroscopy (EIS) is further utilized to investigate the recombination processes of QDSSCs based on the three photoelectrodes. Figure 5 shows the Nyquist curves of the EIS results containing typically two semicircles which are fitted by the equivalent circuit (inset in Figure 5) with the fitted values listed in Table 2, where the electron lifetime can be estimated by $\tau_n' = R_2 \times CEP_2$.[16,44] The simulated data of charge transfer resistance R_1 for the electron transfer process at counter-electrode/electrolyte interface (the first semicircle) is higher than that of DSSCs using I^-/I_3^- electrolyte, ascribed to the low catalytic activity of Pt counter-electrode toward S^{2-}/S_n^{2-} electrolyte.[9,45] At the photoanode/electrolyte interface (the second semicircle), the recombination resistance R_2 exhibits no apparent differences among these three QDSSCs; however, the value of chemical capacitance (CPE_2) of HTS/CdSe QDSSC is larger. As a result, the electron lifetimes τ_n' of these QDSSCs calculated by EIS showed the same order as the IMVS outcomes, although these values are usually larger than that obtained from the latter, since the EIS measurement was performed in the dark.

CONCLUSIONS

The *in situ* electrodeposition method has been shown to ensure high surface coverage of TiO_2 and direct attachment between QDs and TiO_2 matrix when

applied to prepare CdS and/or CdSe QD sensitized hierarchical TiO_2 sphere electrodes. The electron transport and recombination rates in QDSSCs are in the order of HTS/CdS/CdSe > HTS/CdSe ≫ HTS/CdS and HTS/CdS ≈ HTS/CdS/CdSe > HTS/CdSe, respectively, observed by IMPS and IMVS measurements, resulting in a high charge collection efficiency of ~98% for the HTS/CdS/CdSe and HTS/CdSe QDSSCs. Moreover, for HTS/CdS/CdSe QDSSC, higher light harvesting efficiency caused by strong light absorption and better electron injection efficiency ascribed to step-like band gap structure lead to an outstanding η of 4.81% (one sun illumination), which is much higher than that of HTS/CdS (1.01%) or HTS/CdSe (2.69%) QDSSC. The development of near IR absorption QDs and efficient counter-electrode (such as Au, Cu_2S, *etc.*) for the S^{2-}/S_n^{2-} would be expected to enhance the photovoltaic performance of QDSSCs significantly through the present electrodeposition method; this work is now under progress.

EXPERIMENTAL METHODS

Preparation of Hierarchical TiO_2 Sphere (HTS) Electrode. The hierarchical TiO_2 spheres (HTS) were prepared according to a previous method.[33] The solvothermal fabrication of titanium butoxide (TBT) in acetic acid (HAc) was easily carried out at 140 °C for 12 h to give the Ti−complex intermediate. The as-prepared powder was annealed at 500 °C for 3 h to obtain the hierarchical anatase TiO_2 spheres. The HTS paste was screen-printed on a FTO glass (15 Ω/square, Nippon Sheet Glass, Japan) by a developed method.[46] The thickness of TiO_2 films is controlled to be around 15 μm. Before electrodeposition, the TiO_2 films were soaked in 0.04 M aqueous solution of $TiCl_4$ for 30 min at 70 °C, followed by a sintering process at 520 °C for 30 min.

Electrodeposition of CdS and/or CdSe onto HTS. A constant current electrodeposition was carried out to prepare the HTS/CdS, HTS/CdSe, and HTS/CdS/CdSe electrodes. In this process, the HTS-coated FTO glass was used as the work electrode, and a Pt net as the counter electrode.

HTS/CdS Electrode. The electrolyte containing 0.2 M of $Cd(NO)_3$ and 0.2 M of thiourea in a 1/1 (v/v) dimethyl sulphoxide (DMSO)/water was maintained at 90 °C in a water bath. After 25 min of constant current electrodeposition at 0.5 mA cm^{-2}, the HTS/CdS electrode was taken out and washed by deionized water and ethanol successively.

HTS/CdSe or HTS/CdS/CdSe Electrode. The electrolyte was an aqueous solution of 0.02 M of $Cd(CH_3COOH)_2$, 0.04 M of ethylene diamine tetraacetic acid disodium salt (EDTA), and 0.02 M of Na_2SeSO_3 (prepared by refluxing 0.48 g of Se powder and 2.0 g of Na_2SO_3 in water at 100 °C for 3 h), with the solution pH of 7.5−8. The electrodeposition was performed at 0.67 mA cm^{-2} for 45 min on HTS electrode or as-prepared HTS/CdS electrode to get HTS/CdSe or HTS/CdS/CdSe, respectively, followed by washing with water and drying in the open air.

Characterization. The morphologies of HTS, CdS sensitized HTS, and CdS/CdSe cosensitized HTS were characterized by transmission electron microscopy (TEM, JEM2010-HR). The UV−visible absorption spectra of CdS, CdSe sensitized HTS, and CdS/CdSe cosensitized HTS electrodes were measured with the UV−vis−NIR spectrophotometer (Shimadzu UV-3150). The TiO_2 film thickness was measured by a profilometer (Ambios, XP-1).

The as-prepared QD sensitized HTS electrodes can be sandwiched by a Pt-FTO counter-electrode with polysulfide electrolyte filled between. The polysulfide electrolyte contains 1 M of sulfur powder, 1 M of Na_2S and 0.1 M of NaOH dissolved in methanol/water (7:3, v/v). The current density−voltage ($J-V$) measurements were carried out by adopting a Keithley 2400 source meter under simulated AM 1.5 G illumination (100 mW cm^{-2}) provided by a solar simulator (91192, Oriel). A 1 K W xenon arc lamp (6271, Oriel) served as a light source. The incident light intensity was calibrated with a NREL standard Si solar cell. The incident photon-to-current conversion efficiency (IPCE) was recorded on a Keithley 2000 multimeter under the illumination of a 150 W tungsten lamp with a monochromator (Spectral Product DK240). The electrochemical impedance spectroscopy (EIS) measurements were performed on the Zahner Zennium electrochemical workstation, in the dark with an applied bias of −0.5 V. A 10 mV AC sinusoidal signal was employed over the constant bias with the frequency ranging between 1 M Hz and 0.03 Hz. Intensity-modulated photovoltage spectroscopy (IMVS) and intensity-modulated photocurrent spectroscopy (IMPS) spectra were measured on the same electrochemical workstation (Zahner, Zennium) with a frequency response analyzer under an intensity modulated (30−150 W m^{-2}) blue light emitting diode (457 nm) driven by a Zahner (PP211) source supply. The modulated light intensity was 10% or less than the base light intensity. The frequency range was set from 100 KHz to 0.1 Hz.

Acknowledgment. The authors acknowledge the financial supports from the National Natural Science Foundation of China (20873183, 21073239, U0934003), the Fundamental Research Funds for the Central Universities, the Research Fund for the Doctoral Program of Higher Education (20100171110014) and the Research fund of Sun Yat-sen University.

Supporting Information Available: Figure of XRD patterns of CdS and/or CdSe-sensitized TiO_2 films. This material is available free of charge *via* the Internet at http://pubs.acs.org.

REFERENCES AND NOTES

1. Rühle, S.; Shalom, M.; Zaban, A. Quantum-Dot-Sensitized Solar Cells. *Chemphyschem* **2010**, *11*, 2290–2304.
2. Grätzel, M. Photoelectrochemical Cells. *Nature* **2001**, *414*, 338–344.
3. Smith, A. M.; Nie, S. Semiconductor Nanocrystals: Structure, Properties, and Band Gap Engineering. *Acc. Chem. Res.* **2010**, *43*, 190–200.
4. Yu, W. W.; Qu, L. H.; Guo, W. Z.; Peng, X. G. Experimental Determination of the Extinction Coefficient of CdTe, CdSe, and CdS Nanocrystals. *Chem. Mater.* **2003**, *15*, 2854–2860.
5. Wang, P.; Zakeeruddin, S. M.; Moser, J. E.; Humphry-Baker, R.; Comte, P.; Aranyos, V.; Hagfeldt, A.; Nazeeruddin, M. K.; Grätzel, M. Stable New Sensitizer with Improved Light Harvesting for Nanocrystalline Dye-Sensitized Solar Cells. *Adv. Mater.* **2004**, *16*, 1806–1811.
6. Sambur, J. B.; Novet, T.; Parkinson, B. A. Multiple Exciton Collection in a Sensitized Photovoltaic System. *Science* **2010**, *330*, 63–66.
7. Klimov, V. I. Mechanisms for Photogeneration and Recombination of Multiexcitons in Semiconductor Nanocrystals: Implications for Lasing and Solar Energy Conversion. *J. Phys. Chem. B* **2006**, *110*, 16827–16845.
8. Mora-Seró, I.; Bisquert, J. Breakthroughs in the Development of Semiconductor-Sensitized Solar Cells. *J. Phys. Chem. Lett.* **2010**, *1*, 3046–3052.
9. Lee, Y. L.; Lo, Y. S. Highly Efficient Quantum-Dot-Sensitized Solar Cell Based on Co-Sensitization of CdS/CdSe. *Adv. Funct. Mater.* **2009**, *19*, 604–609.
10. Seol, M.; Kim, H.; Tak, Y.; Yong, K. Novel Nanowire Array Based Highly Efficient Quantum Dot Sensitized Solar Cell. *Chem. Commun.* **2010**, *46*, 5521–5523.
11. Zhang, Q. X.; Guo, X. Z.; Huang, X. M.; Huang, S. Q.; Li, D. M.; Luo, Y. H.; Shen, Q.; Toyoda, T.; Meng, Q. B. Highly Efficient CdS/CdSe-Sensitized Solar Cells Controlled by the Structural

Properties of Compact Porous TiO_2 Photoelectrodes. *Phys. Chem. Chem. Phys.* **2011**, *13*, 4659–4667.
12. Niitsoo, O.; Sarkar, S. K.; Pejoux, C.; Rühle, S.; Cahen, D.; Hodes, G. Chemical Bath Deposited CdS/CdSe-Sensitized Porous TiO_2 Solar Cells. *J. Photochem. Photobiol. A* **2006**, *181*, 306–313.
13. Giménez, S.; Lana-Villarreal, T.; Gómez, R.; Agouram, S.; Muñoz-Sanjosé, V.; Mora-Seró, I. Determination of Limiting Factors of Photovoltaic Efficiency in Quantum Dot Sensitized Solar Cells: Correlation between Cell Performance and Structural Properties. *J. Appl. Phys.* **2010**, *108*, 064310.
14. Diguna, L. J.; Shen, Q.; Kobayashi, J.; Toyoda, T. High Efficiency of CdSe Quantum-Dot-Sensitized TiO_2 Inverse Opal Solar Cells. *Appl. Phys. Lett.* **2007**, *91*, 023116.
15. Lee, H.; Wang, M. K.; Chen, P.; Gamelin, D. R.; Zakeeruddin, S. M.; Grätzel, M.; Nazeeruddin, M. K. Efficient CdSe Quantum Dot-Sensitized Solar Cells Prepared by an Improved Successive Ionic Layer Adsorption and Reaction Process. *Nano Lett.* **2009**, *9*, 4221–4227.
16. Mora-Seró, I.; Giménez, S.; Fabregat-Santiago, F.; Gómez, R.; Shen, Q.; Toyoda, T.; Bisquert, J. Recombination in Quantum Dot Sensitized Solar Cells. *Acc. Chem. Res.* **2009**, *42*, 1848–1857.
17. Watson, D. F. Linker-Assisted Assembly and Interfacial Electron-Transfer Reactivity of Quantum Dot–Substrate Architectures. *J. Phys. Chem. Lett.* **2010**, *1*, 2299–2309.
18. Park, Y. S.; Dmytruk, A.; Dmitruk, I.; Kasuya, A.; Takeda, M.; Ohuchi, N.; Okamoto, Y.; Kaji, N.; Tokeshi, M.; Baba, Y. Size-Selective Growth and Stabilization of Small CdSe Nanoparticles in Aqueous Solution. *ACS Nano* **2010**, *4*, 121–128.
19. Robel, I.; Subramanian, V.; Kuno, M.; Kamat, P. V. Quantum Dot Solar Cells. Harvesting Light Energy with CdSe Nanocrystals Molecularly Linked to Mesoscopic TiO_2 Films. *J. Am. Chem. Soc.* **2006**, *128*, 2385–2393.
20. Acharya, K. P.; Khon, E.; O'Conner, T.; Nemitz, I.; Klinkova, A.; Khnayzer, R. S.; Anzenbacher, P.; Zamkov, M. Heteroepitaxial Growth of Colloidal Nanocrystals onto Substrate Films *via* Hot-Injection Routes. *ACS Nano* **2011**, *5*, 4953–4964.
21. Yu, X. Y.; Lei, B. X.; Kuang, D. B.; Su, C. Y. Highly Efficient CdTe–CdS Quantum Dot Sensitized Solar Cells Fabricated by a One-Step Linker Assisted Chemical Bath Deposition. *Chem. Sci.* **2011**, *2*, 1396–1400.
22. Wang, X. N.; Zhu, H. J.; Xu, Y. M.; Wang, H.; Tao, Y.; Hark, S.; Xiao, X. D.; Li, Q. A. Aligned ZnO/CdTe Core–Shell Nanocable Arrays on Indium Tin Oxide: Synthesis and Photoelectrochemical Properties. *ACS Nano* **2010**, *4*, 3302–3308.
23. Myung, Y.; Jang, D. M.; Sung, T. K.; Sohn, Y. J.; Jung, G. B.; Cho, Y. J.; Kim, H. S.; Park, J. Composition-Tuned ZnO–CdSSe Core–Shell Nanowire Arrays. *ACS Nano* **2010**, *4*, 3789–3800.
24. Spurgeon, J. M.; Atwater, H. A.; Lewis, N. S. A Comparison Between the Behavior of Nanorod Array and Planar Cd(Se, Te) Photoelectrodes. *J. Phys. Chem. C* **2008**, *112*, 6186–6193.
25. Hyun, B. R.; Zhong, Y. W.; Bartnik, A. C.; Sun, L. F.; Abruña, H. D.; Wise, F. W.; Goodreau, J. D.; Matthews, J. R.; Leslie, T. M.; Borrelli, N. F. Electron Injection from Colloidal PbS Quantum Dots into Titanium Dioxide Nanoparticles. *ACS Nano* **2008**, *2*, 2206–2212.
26. Robel, I.; Kuno, M.; Kamat, P. V. Size-Dependent Electron Injection from Excited CdSe Quantum Dots into TiO_2 Nanoparticles. *J. Am. Chem. Soc.* **2007**, *129*, 4136–4137.
27. Martínez-Ferrero, E.; Mora-Seró, I.; Albero, J.; Giménez, S.; Bisquert, J.; Palomares, E. Charge Transfer Kinetics in CdSe Quantum Dot Sensitized Solar Cells. *Phys. Chem. Chem. Phys.* **2010**, *12*, 2819–2821.
28. González-Pedro, V.; Xu, X. Q.; Mora-Seró, I.; Bisquert, J. Modeling High-Efficiency Quantum Dot Sensitized Solar Cells. *ACS Nano* **2010**, *4*, 5783–5790.
29. Liu, W. Q.; Hu, L. H.; Dai, S. Y.; Guo, L.; Jiang, N. Q.; Kou, D. X. The Effect of The Series Resistance in Dye-Sensitized Solar Cells Explored by Electron Transport and Back Reaction Using Electrical and Optical Modulation Techniques. *Electrochim. Acta* **2010**, *55*, 2338–2343.
30. Zhu, K.; Vinzant, T. B.; Neale, N. R.; Frank, A. J. Removing Structural Disorder from Oriented TiO_2 Nanotube Arrays: Reducing the Dimensionality of Transport and Recombination in Dye-Sensitized Solar Cells. *Nano Lett.* **2007**, *7*, 3739–3746.
31. Schlichthorl, G.; Park, N. G.; Frank, A. J. Evaluation of the Charge-Collection Efficiency of Dye-Sensitized Nanocrystalline TiO_2 Solar Cells. *J. Phys. Chem. B* **1999**, *103*, 782–791.
32. Dloczik, L.; Ileperuma, O.; Lauermann, I.; Peter, L. M.; Ponomarev, E. A.; Redmond, G.; Shaw, N. J.; Uhlendorf, I. Dynamic Response of Dye-Sensitized Nanocrystalline Solar Cells: Characterization by Intensity-Modulated Photocurrent Spectroscopy. *J. Phys. Chem. B* **1997**, *101*, 10281–10289.
33. Liao, J. Y.; Lei, B. X.; Kuang, D. B.; Su, C. Y. Tri-Functional Hierarchical TiO_2 Spheres Consisting of Anatase Nanorods and Nanoparticles for High Efficiency Dye-Sensitized Solar Cells. *Energy Environ. Sci.* **2011**, *4*, 4079–4085.
34. Wong, D. K. P.; Ku, C. H.; Chen, Y. R.; Chen, G. R.; Wu, J. J. Enhancing Electron Collection Efficiency and Effective Diffusion Length in Dye-Sensitized Solar Cells. *Chemphyschem* **2009**, *10*, 2698–2702.
35. Martinson, A. B. F.; Goes, M. S.; Fabregat-Santiago, F.; Bisquert, J.; Pellin, M. J.; Hupp, J. T. Electron Transport in Dye-Sensitized Solar Cells Based on ZnO Nanotubes: Evidence for Highly Efficient Charge Collection and Exceptionally Rapid Dynamics. *J. Phys. Chem. A* **2009**, *113*, 4015–4021.
36. Hsiao, P. T.; Tung, Y. L.; Teng, H. S. Electron Transport Patterns in TiO_2 Nanocrystalline Films of Dye-Sensitized Solar Cells. *J. Phys. Chem. C* **2010**, *114*, 6762–6769.
37. Krüger, J.; Plass, R.; Grätzel, M.; Cameron, P. J.; Peter, L. M. Charge Transport and Back Reaction in Solid-State Dye-Sensitized Solar Cells: A Study Using Intensity-Modulated Photovoltage and Photocurrent Spectroscopy. *J. Phys. Chem. B* **2003**, *107*, 7536–7539.
38. Bang, J. H.; Kamat, P. V. Quantum Dot Sensitized Solar Cells. A Tale of Two Semiconductor Nanocrystals: CdSe and CdTe. *ACS Nano* **2009**, *3*, 1467–1476.
39. Van de Walle, C. G.; Neugebauer, J. Universal Alignment of Hydrogen Levels in Semiconductors, Insulators and Solutions. *Nature* **2003**, *423*, 626–628.
40. Ellis, A. B.; Kaiser, S. W.; Bolts, J. M.; Wrighton, M. S. Study of n-Type Semiconducting Cadmium Chalcogenide-Based Photoelectrochemical Cells Employing Polychalcogenide Electrolytes. *J. Am. Chem. Soc.* **1977**, *99*, 2839–2848.
41. Hodes, G. Comparison of Dye- and Semiconductor-Sensitized Porous Nanocrystalline Liquid Junction Solar Cells. *J. Phys. Chem. C* **2008**, *112*, 17778–17787.
42. Hagfeldt, A.; Boschloo, G.; Sun, L. C.; Kloo, L.; Pettersson, H. Dye-Sensitized Solar Cells. *Chem. Rev.* **2010**, *110*, 6595–6663.
43. Zhu, K.; Neale, N. R.; Miedaner, A.; Frank, A. J. Enhanced Charge-Collection Efficiencies and Light Scattering in Dye-Sensitized Solar Cells Using Oriented TiO_2 Nanotubes Arrays. *Nano Lett.* **2007**, *7*, 69–74.
44. Fabregat-Santiago, F.; Bisquert, J.; Garcia-Belmonte, G.; Boschloo, G.; Hagfeldt, A. Influence of Electrolyte in Transport and Recombination in Dye-Sensitized Solar Cells Studied by Impedance Spectroscopy. *Sol. Energy Mater. Sol. Cells* **2005**, *87*, 117–131.
45. Mora-Seró, I.; Giménez, S.; Moehl, T.; Fabregat-Santiago, F.; Lana-Villareal, T.; Gómez, R.; Bisquert, J. Factors Determining the Photovoltaic Performance of a CdSe Quantum Dot Sensitized Solar Cell: The Role of the Linker Molecule and of the Counter-Electrode. *Nanotechnology* **2008**, *19*, 424007.
46. Lei, B. X.; Fang, W. J.; Hou, Y. F.; Liao, J. Y.; Kuang, D. B.; Su, C. Y. All-Solid-State Electrolytes Consisting of Ionic Liquid and Carbon Black for Efficient Dye-Sensitized Solar Cells *J. Photochem. Photobiol. A* **2010**, *216*, 8–14.